Supplemental material

Figure S1

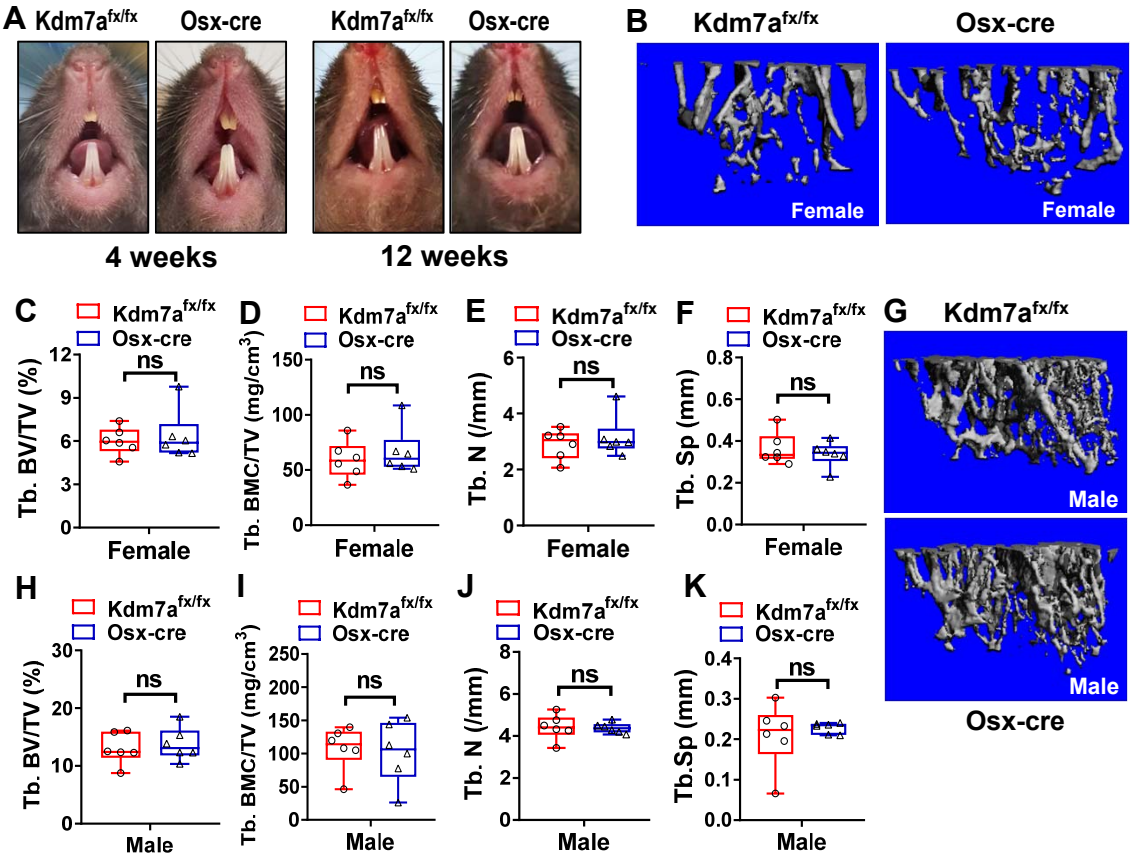

Figure S1. Osx-Cre mice did not show dental and skeletal defects. Gross appearance of incisors in 4-week-old and 12-week-old mice was shown (A). μCT analyses were performed on the tibial metaphyseal bone of 24-week-old female (B-F) and male (G-K) mice. The reconstruction images are shown (B, G). Histomorphometric parameters were analyzed in female (C-F) and male (H-K) mice. Data are presented as box-and-whiskers plots, n=6. Student's t test was performed for statistical analyses, ns: no significance.

Figure S2

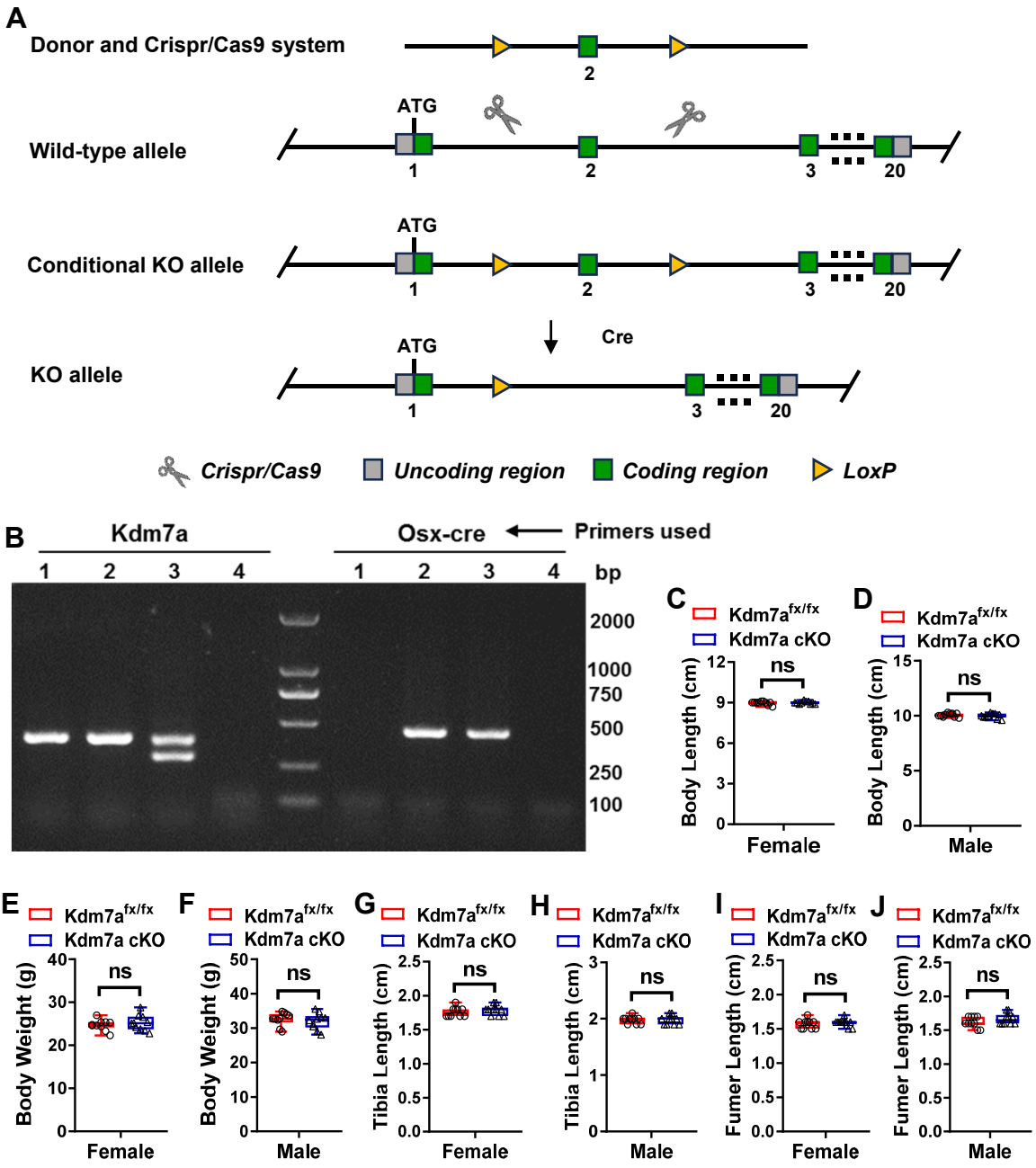

Figure S2. Kdm7a cKO mice did not show abnormalities in body length, weight and bone length. The strategy for making Kdm7a cKO mice is shown (A). The genotypes of the mutant mice were confirmed by genotyping PCR (B). Lables 1: Kdm7a$^{fx/fx}$; 2: Kdm7a cKO; 3: Positive control; 4: Negative control. (C-J) Measurements of body length (total length minus that of the tail), weight and bone length. Data are presented as box-and-whiskers plots, n=10. Student's t test was performed for statistical analyses, ns: no significance.

Figure S3

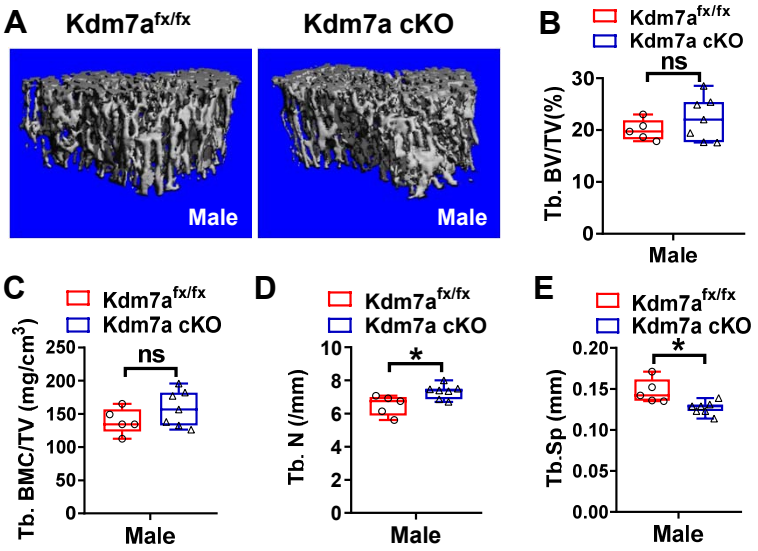

Figure S3. Cancellous bone mass was not changed in 12-week-old Kdm7a mice. μCT analyses were performed on the cancellous bone architecture in the proximal tibial metaphysis of 12-week-old male mice. The reconstruction images are shown (A). Histomorphometric parameters were analyzed on cancellous bone (B-E). Data are presented as box-and-whiskers plots, n=5~7. Comparisons were conducted using Student's t test. *p < 0.05, ns: no significance.

Figure S4

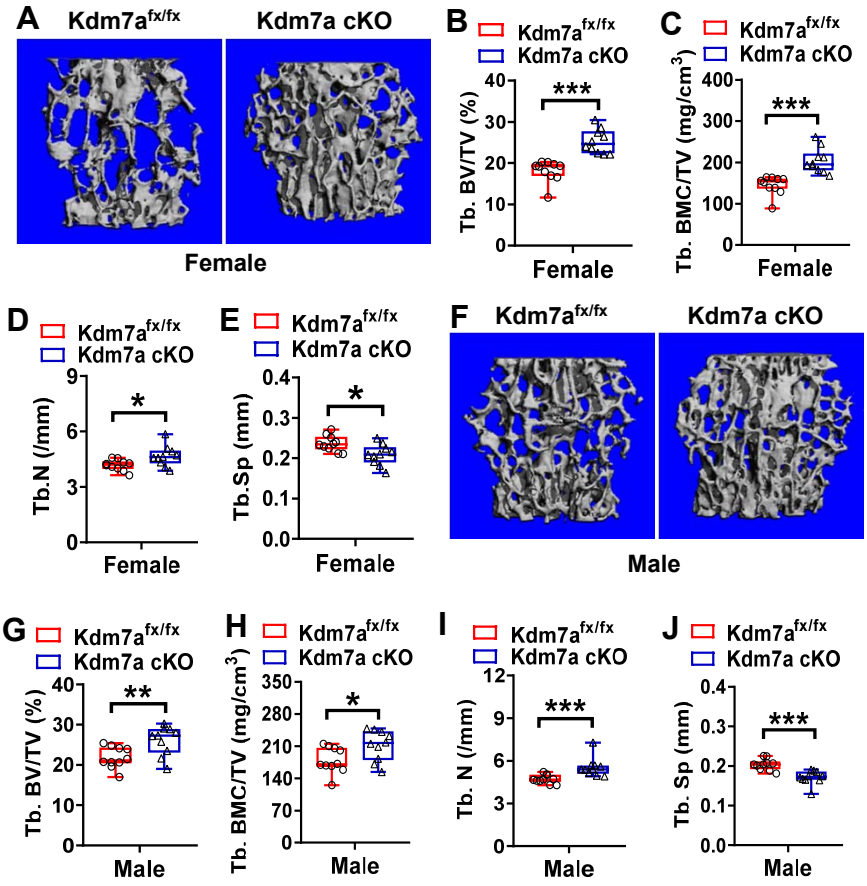

Figure S4. Deletion of Kdm7a in osteoprogenitor cells promoted bone mass accrual in lumbar vertebrae of mice. µCT analyses were performed on the bone architecture in the L2 Lumbar vertebrae of 24-week-old female (A-E) and male (F-J) mice. The reconstruction images are shown (A: female; F: male). Histomorphometric parameters were analyzed on cancellous bone in female (B-E) and male (G-J) mice. Data are presented as box-and-whiskers plots, n=10. Student's t test was performed for statistical analyses. *p < 0.05, **p < 0.01, ***p < 0.001.

Figure S5

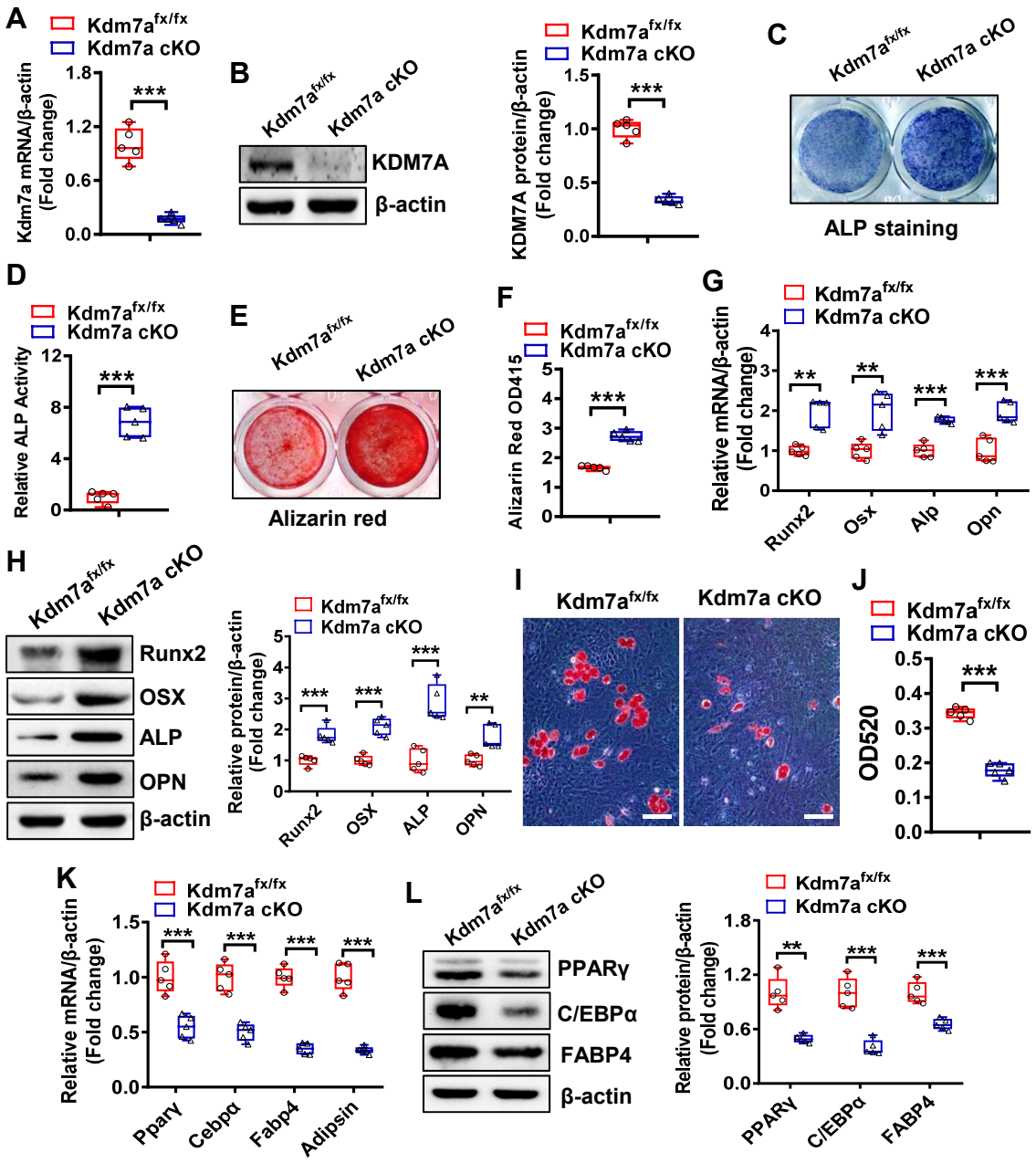

Figure S5. Differentiation was dysregulated in pre-osteoblastic cells from Kdm7a cKO mice. RT-qPCR and Western blotting were performed to verify the deletion of Kdm7a in calvarial pre-osteoblastic cells from the Kdm7a cKO mice (A, B). Fourteen days after osteogenic treatment, ALP staining was performed (C) and ALP activity (D) was measured. Twenty one days after osteogenic induction, alizarin red staining was performed (E) and the intensity of staining was quantified (F). The mRNA (G) and protein (H) levels of osteogenic factors were detected 72 h after induction by RT-qPCR and Western blotting, respectively. Five days after adipogenic induction, oil red O staining was performed (I) and the quantity of dye accumulation in the cells was measured (J). The mRNA (K) and protein (L) levels of adipogenic factors were examined 48 h and 72 h respectively after induction. Image scale in (I): 100 μm. Data are presented as box-and-whiskers plots, n=5. Comparisons were conducted using Student's t test. **p < 0.01, ***p < 0.001.

Figure S6

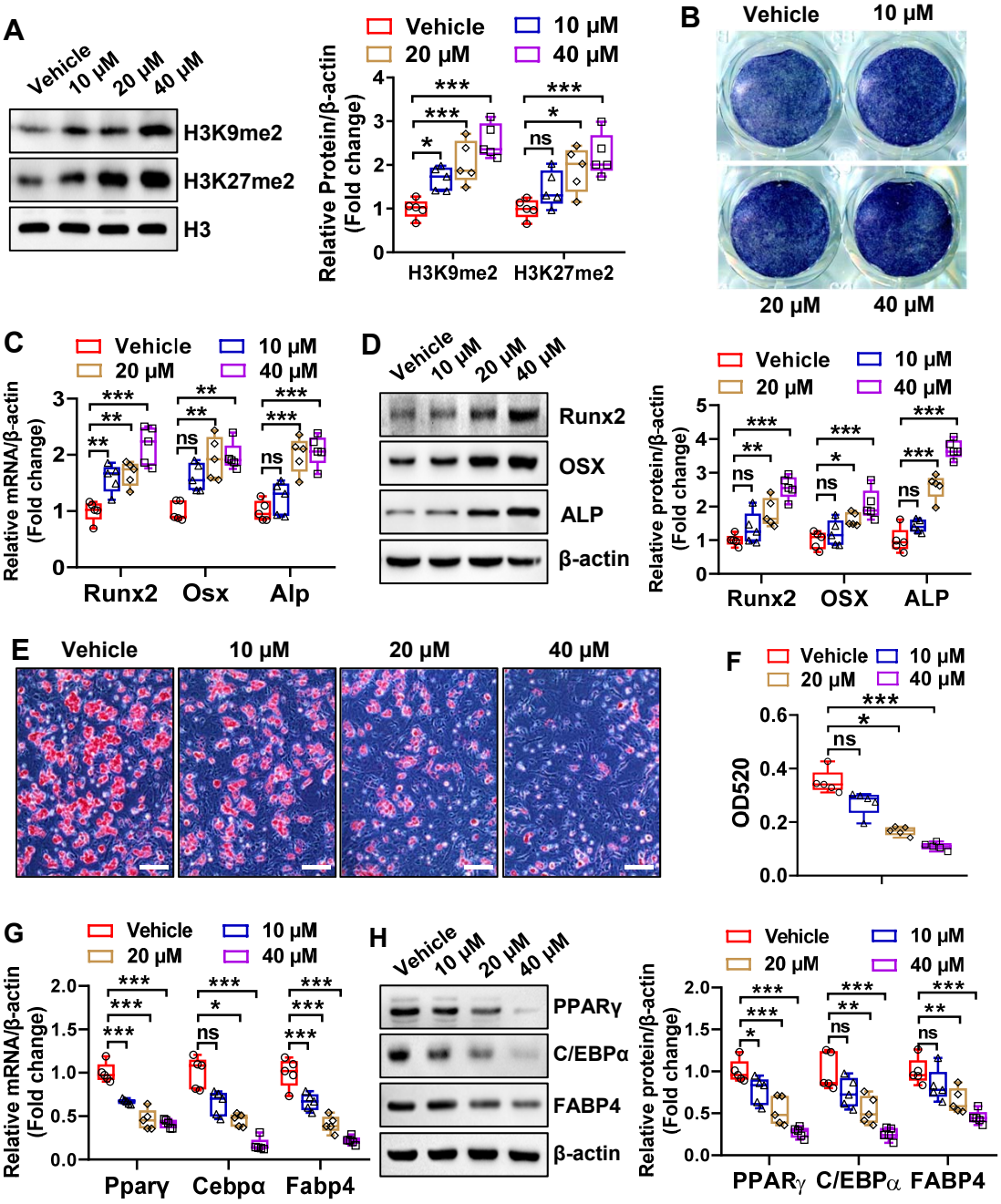

Figure S6. TC-E 5002 treatment promoted osteoblast differentiation and blocked adipocyte formation from BMSCs. BMSCs was treated with different doses of TC-E 5002 and the levels of H3K9me2 and H3K27me3 were examined using Western blotting (A). Fourteen days after osteogenic treatment, ALP staining was performed (B). The mRNA (C) and protein (D) levels of osteogenic factors were measured 72 h after induction by RT-qPCR and Western blotting, respectively. Five days after adipogenic induction, oil red O staining was performed (E) and the quantity of dye accumulation in the cells was measured (F). The mRNA (G) and protein (H) levels of adipogenic factors were examined 48 h and 72 h respectively after induction. Image scale in (E): 100 μm. Data are presented as box-and-whiskers plots, n=5. Comparisons were conducted using One-way ANOVA followed by Dunnett'stest.*p < 0.05, **p < 0.01, ***p < 0.001, ns: no significance.

Figure S7

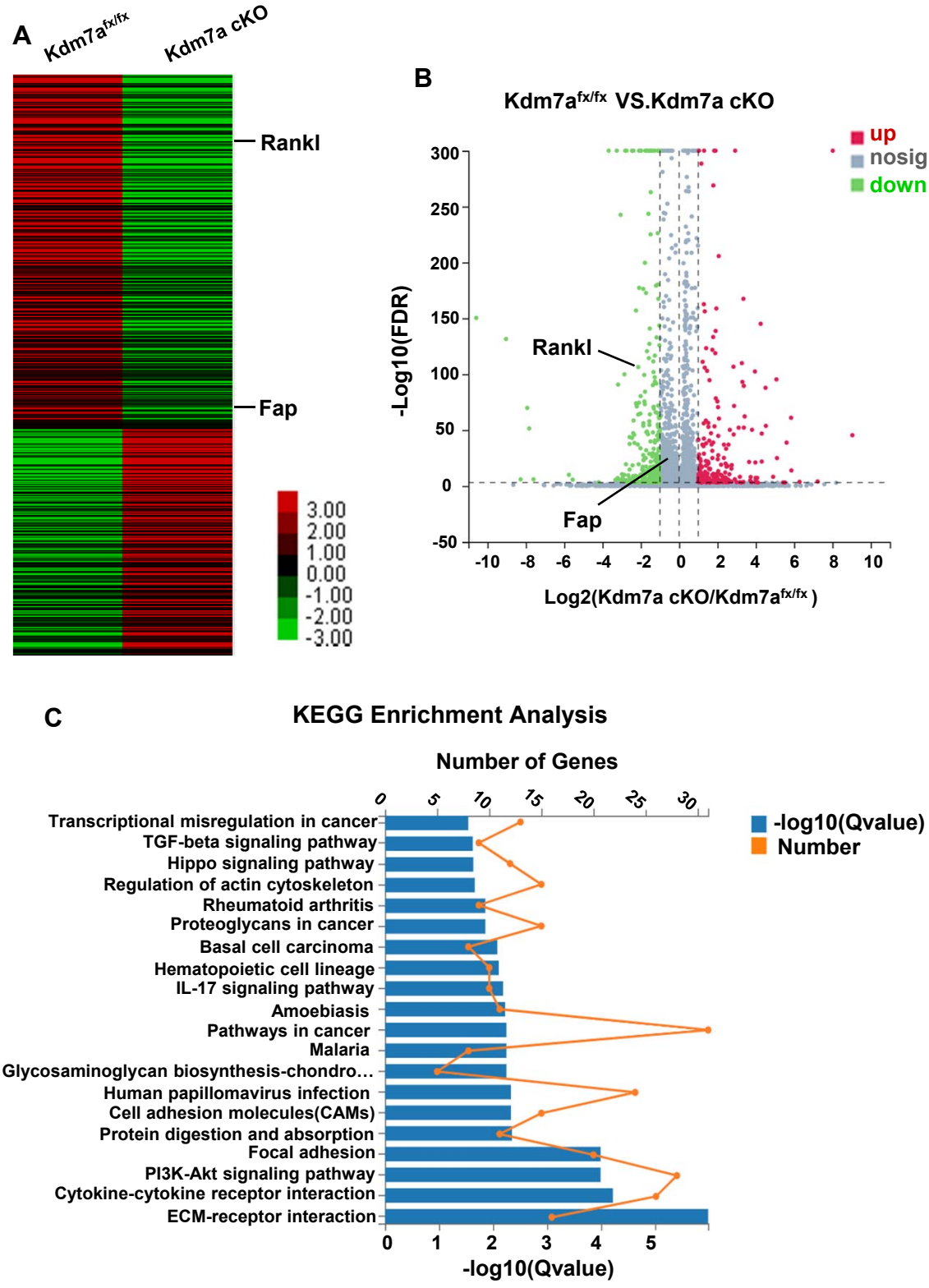

Figure S7. RNA-seq revealed differentially expressed genes in calvarial pre-osteoblastic cells derived from Kdm7a cKO and Kdm7a$^{fx/fx}$ mice. The differentially expressed genes in calvarial pre-osteoblastic cells derived from Kdm7a cKO and Kdm7a$^{fx/fx}$ control mice are shown (A). Q adjust and fold change >2 are set as restrictive conditions to identify the differentially expressed genes (B). KEGG enrichment analysis of related pathways were done and the top-ranking enriched pathways are shown (C).

Figure S8

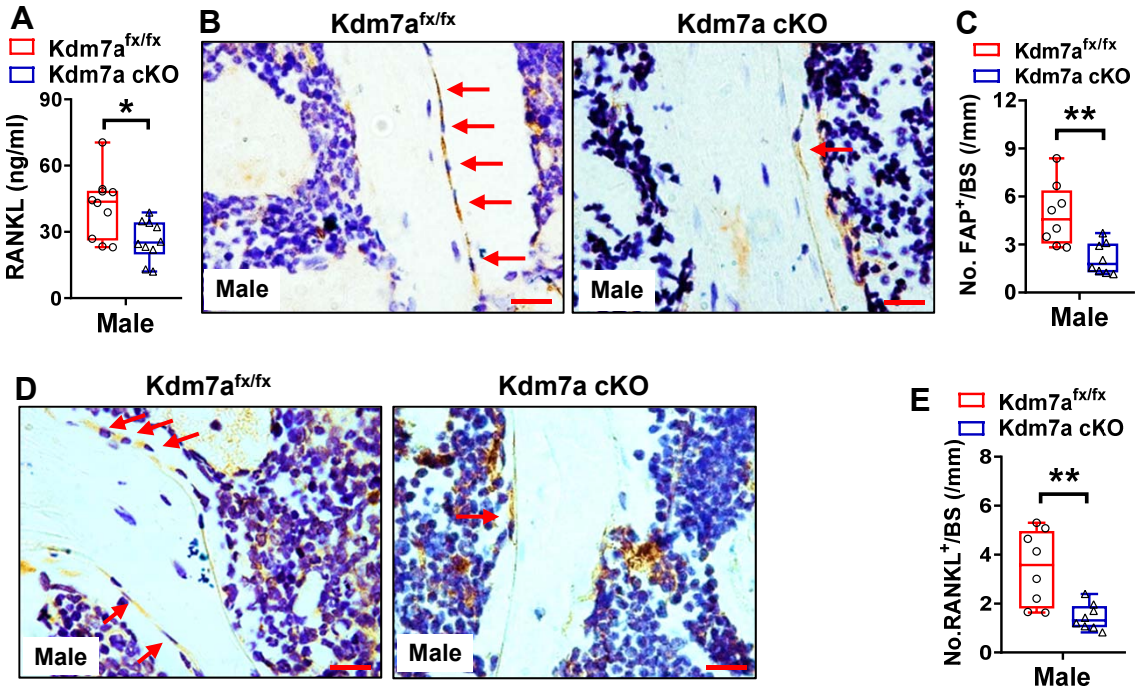

Figure S8. Kdm7a deletion in osteoprogenitor cells downregulated FAP and RANKL expression in male mice. Serum RANKL levels were measured in 24-week-old male mice using ELISA (A). IHC staining of FAP and RANKL was performed (B, D). FAP-positive cells and RANKL-positive cells on trabeculae were counted (C, E) . Image scale in (B,D): 20 μm. Data are presented as box-and-whiskers plots, n=10 in (A); n=8 in (C, E). Comparisons were conducted using Student's t test. *$p < 0.05$, **$p < 0.01$.

Figure S9

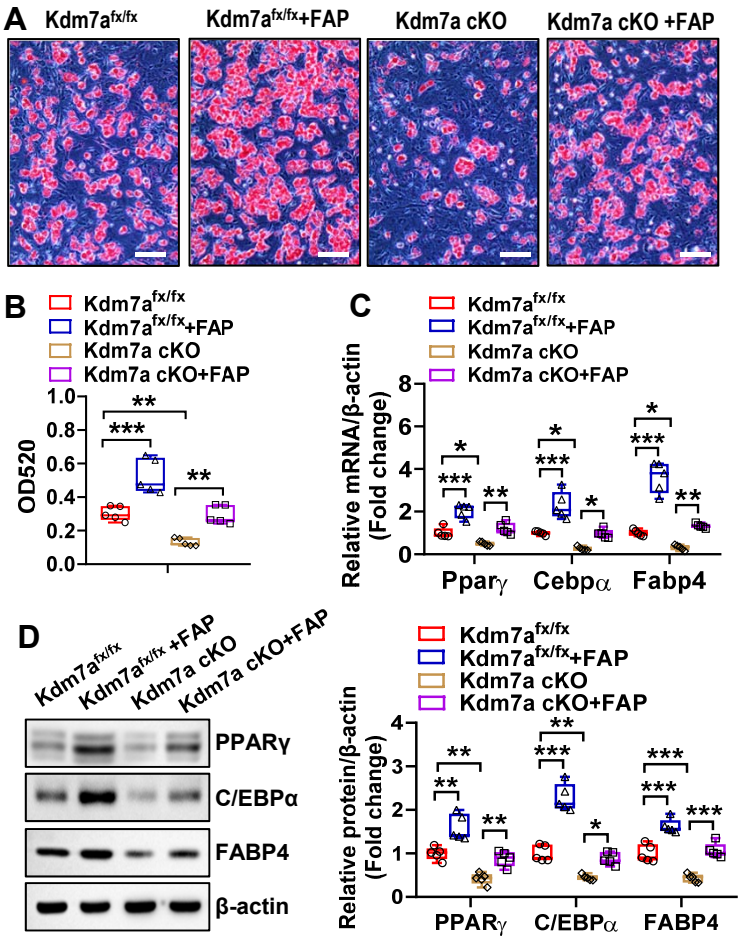

Figure S9. FAP attenuated Kdm7a deletion-induced dysregulation of adipogenic differentiation. Primary BMSCs were cultured, and treated with recombinant FAP followed by adipogenic induction. Oil red O staining was performed 5 days after adipogenic induction and the quantity of oil red O accumulation in cells was measured (A, B). The mRNA (C) and protein (D) levels of adipogenic factors were measured 72 h after adipogenic induction. Image scale in (A): 100 μm. Data are presented as box-and-whiskers plots, n=5. Comparisons were conducted using two-way ANOVA followed by Tukey's test. *p < 0.05, **p < 0.01, ***p < 0.001.

Supplemental Table S1. Primers used for Genotyping, RT-PCR and ChIP assays

Genes	Forward primer sequences	Reverse primer sequences
Kdm7a genotyping	CAATGCCAGATAAGTGCTGGCTAG	CTGGCATTACTGACCTAAGCGC
Osx-Cre genotyping	TACCAGAAGCGACCACTTGAGC	GCACACAGACAGGAGCATCTTC
PPARγ	CTTGACAGGAAAGACAACGG	GCTTCTACGGATCGAAACTG
C/EBPα	CTGATTCTTGCCAAACTGAG	GAGGAAGCTAAGACCCACTAC
Fabp4	AAATCACCGCAGACGACAGG	GGCTCATGCCCTTTCATAAAC
adipsin	TGATGTGTGCAGAGAGCAAC	CGTAACCACACCTTCGACTG
Runx2	TCCTGTAGATCCGAGCACCA	CTGCTGCTGTTGTTGCTGTT
Alp	CCAGAAAGACACCTTGACTGTGG	TCTTGTCCGTGTCGCTCACCAT
Osterix	GGCTTTTCTGCGGCAAGAGGTT	CGCTGATGTTTGCTCAAGTGGTC
Osteocalcin	GCAATAAGGTAGTGAACAGACTCC	CCATAGATGCGTTTGTAGGCGG
Kdm7a	GATCGAGTGCGATGTCTGCAAG	TTAAGGAAGAGCCGTGTAGAGCTG
Rankl	GTGAAGACACACTACCTGACTCC	GCCACATCCAACCATGAGCCTT
Fap	CCGCGTAACACAGGATTCACTG	CACACTTCTTGCTCGGAGGAGA
β-actin	AAGACCTCTATGCCAACACAG	GGAGGAGCAATGATCTTGATC
Rankl (ChIP)	AGGCTATATTTGGAGGGATAACTG	CTCTAGTGAACTCCGTCCGAAGCC
Rankl (ChIP) Ctrl	GGCTTAGATGATCCTTCTATTGGC	CACAGAAAGATGTATGCCGTTATT
Fap (ChIP)	CCCAAACATTTGATATGTACAATG	ATCACTCGAGTCACTTTAGTAACA
Fap (ChIP) Ctrl	GGCAGAAAAGCTAATGTGCTGCAC	TAACTTTTGGGAGGGTGAGTTTTT

Supplemental Table S2. Primary antibodies for Western blotting

Antibody	Catalog number	Brand
anti-Runx2	ab192256	Abcam (Cambridge, MA, USA)
anti-low-density lipoprotein receptor-related protein 6 (LRP6)	ab134146	
anti-KDM7A	A8266	Abclonal (Wuhan, China)
anti-β-actin	AC026	
anti-nuclear factor of activated T cells 1 (NFATc1)	A1539	
anti-cathepsin K (CTSK)	A1782	
anti-osterix	DF7713	Affinity (Changzhou, China)
anti-non-phospho-β-catenin	#8814	Cell Signaling Technology (Danvers, MA, USA)
anti-C/EBPα	#8178	
anti-PPARγ	#2443	
anti-phospho-LRP6 (Ser1490)	#2568	
anti-ALP	(ET1601-21)	Huabio (Hangzhou, China)
anti-fatty acid binding protein 4 (FABP4)	67167-1-Ig	Proteintech (Wuhan, China)
anti-osteopontin	22952-1-AP	
anti-glycogen synthase kinase 3β (GSK3β)	24198-1-AP	
anti-phospho-GSK3β (S9)	67558-1-Ig	
anti-β-catenin	66379-1-Ig	
anti-RANKL	WL00285	Wanleibio (Shenyang, China)
anti-fibroblast activation protein α (FAP)	WL04890	